Brain Proton Magnetic Resonance Spectroscopy
Introduction and Overview

Débora Bertholdo, MD, Arvemas Watcharakorn, MD,
Mauricio Castillo, MD*

KEYWORDS

• ^{1}H Magnetic resonance spectroscopy • Stimulated echo acquisition mode • Brain metabolites
• Brain tumors

KEY POINTS

- Magnetic resonance (MR) proton spectroscopy is a technique which mainly provides biological information regarding cellularity, energy, neuron viability, necrosis and ischemia.
- MR spectroscopy is ideal to assess the limits of brain tumors when planning surgery.
- MR spectroscopy allows identification of some metabolic disorders guiding further laboratory analysis.

INTRODUCTION

Magnetic resonance (MR) spectroscopy is an analytical method used in chemistry that enables the identification and quantification of metabolites in samples. It differs from conventional MR imaging in that spectra provide physiologic and chemical information instead of anatomy.

MR spectroscopy and MR imaging have their origin in nuclear magnetic resonance (NMR). NMR was first described in 1946 simultaneously by the Nobel Prize winners Edward Purcell, from Harvard University, and Felix Bloch, from Stanford University. At that time, NMR was used only by physicists for purposes of determining the nuclear magnetic moments of nuclei. It was only in the mid 1970s that NMR started to be used in vivo, after Lauterbur, Mansfield, and Grannell introduced gradient into the magnetic field, enabling them to determine the location of the emitted signal and to reproduce it on an image. In vivo NMR was renamed MR imaging because the term "nuclear" had been consistently (but erroneously) associated with nuclear medicine. For the same reason, NMR spectroscopy used in vivo is now named MR spectroscopy. During the 1980s, the first MR imaging medical scanners became available for clinical use. Since then improvements have been made, especially in relation to higher field strengths.

MR spectra may be obtained from different nuclei. Protons (^{1}H) are the nuclei most used for clinical applications in the human brain, mainly because of their high sensitivity and abundance. The proton MR spectrum is altered in almost all neurologic disorders. In some diseases, proton MR spectroscopy (^{1}H-MRS) changes are very subtle and are not reliable without a statistical comparison between groups of patients. In these cases, ^{1}H-MRS is usually used for research. In clinical practice, ^{1}H-MRS is mostly used for more detailed analysis of primary and secondary brain tumors and metabolic diseases.

This article discusses the physical basis of ^{1}H-MRS, emphasizing the different techniques, the normal spectra in adults and children, its clinical applications, and the significance of brain

University of North Carolina at Chapel Hill, Room 3326 Old Infirmary Building, Manning Drive, Chapel Hill, NC 27599, USA
* Corresponding author.
E-mail address: castillo@med.unc.edu

Neuroimag Clin N Am 23 (2013) 359–380
http://dx.doi.org/10.1016/j.nic.2012.10.002
1052-5149/13/$ – see front matter

metabolites under both normal and abnormal conditions, particularly in the evaluation of brain tumors.

PHYSICAL BASIS

Many nuclei may be used to obtain MR spectra, including phosphorus (^{31}P), fluorine (^{19}F), carbon (^{13}C), and sodium (^{23}Na). The ones mostly used for clinical MR spectroscopy are protons (^{1}H). The brain is ideally imaged with ^{1}H-MRS because of its near lack of motion (this prevents MR spectroscopy from being used in the abdomen and thorax without very sophisticated motion-reduction techniques). The hydrogen nucleus is abundant in human tissues. ^{1}H-MRS requires only standard radiofrequency (RF) coils and a dedicated software package. For nonproton MR spectroscopy, RF coils tuned to the Larmor frequency of other nuclei, matching preamplifiers, hybrids, and a broadband power amplifier are needed.

Different field strengths are used for conventional clinical MR imaging, ranging from 0.2 to 3 T. Because the main objective of ^{1}H-MRS is to detect weak signals from metabolites, a minimum of 1.5 T is advised. Units with higher field strength have the advantage of higher signal-to-noise ratio (SNR), better resolution, and shorter acquisition times, making the technique useful in sick patients and others who cannot hold still for long periods of time.

^{1}H-MRS is based on the chemical-shift properties of the atom. When a tissue is exposed to an external magnetic field, its nuclei will resonate at a frequency (f) that is given by the Larmor equation:

$$f = \gamma B_0$$

Because the gyromagnetic ratio (γ) is a constant of each nuclear species, the spin frequencies of certain nuclei (f) depend on the external magnetic field (B_0) and the local microenvironment. The electric shell interactions of these nuclei with the surrounding molecules cause a change in the local magnetic field, leading to a change on the spin frequency of the atom (a phenomenon called chemical shift). The value of this difference in resonance frequency gives information about the molecular group carrying ^{1}H and is expressed in parts per million (ppm). The chemical-shift position of a nucleus is ideally expressed in ppm because it is independent of the field strength (choline, for example, will be positioned at 3.22 ppm at 1.5 or 7 T). The MR spectrum is represented by the x axis that corresponds to the metabolite frequency in ppm according to the chemical shift, and the y axis that corresponds to the peak amplitude.

Some metabolites such as lactate have doublets, triplets, or multiplets instead of single peaks. These peaks are broken down into more complex peaks and are explained by J-coupling, also named spin-spin coupling. The J-coupling phenomenon occurs when the molecular structure of a metabolite is such that protons are found in different atomic groups (eg, CH_3- and CH_2-). These groups have slightly different local magnetic fields, thus each ^{1}H resonates at a frequency that is characteristic of its position in the molecule, resulting in a multiplet peak.

Techniques

The ^{1}H-MRS acquisition usually starts with anatomic images, which are used to select a volume of interest (VOI), where the spectrum will be acquired. For the spectrum acquisition, different techniques may be used, including single-voxel and multi-voxel imaging using both long and short echo times (TE). Each technique has advantages and disadvantages, and choosing the right one for a specific purpose is important in improving the quality of the results.

Single-voxel spectroscopy

In single-voxel spectroscopy (SVS) the signal is obtained from a voxel previously selected. This voxel is acquired from a combination of slice-selective excitations in 3 dimensions in space, achieved when an RF pulse is applied while a field gradient is switched on. It results in 3 orthogonal planes whose intersection corresponds to the VOI (Fig. 1).

One of two techniques is typically used for acquisition of SVS ^{1}H-MRS spectra: pointed-resolved spectroscopy (PRESS) and stimulated

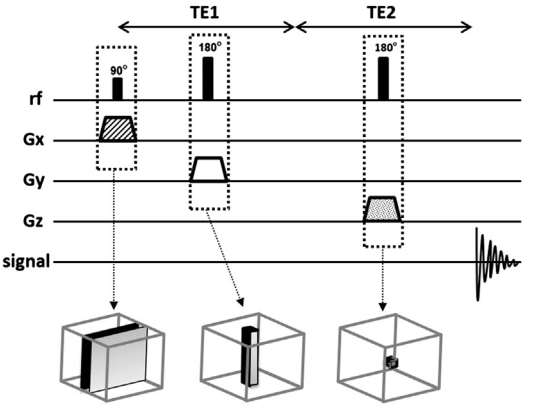

Fig. 1. Slice selection in single-voxel spectroscopy. The 3 radiofrequency pulses (rf) select 3 orthogonal planes (Gz, Gy, and Gx). Their intersection corresponds to the volume of interest (VOI). TE, echo time.

echo acquisition mode (STEAM). The most used SVS technique is PRESS. In the PRESS sequence, the spectrum is acquired using 1 90° pulse followed by 2 180° pulses, each of which is applied at the same time as a different field gradient. Thus, the signal emitted by the VOI is a spin echo. The first 180° pulse is applied after time TE1/2 from the first pulse (90° pulse), and the second 180° is applied after time TE1/2 + TE. The signal occurs after a time 2TE (**Fig. 2**). To restrict the acquired sign to the selected VOI, spoiler gradients are needed. Spoiler gradients dephase the nuclei outside the VOI and reduce their signal.

STEAM is the second most commonly used SVS technique. In this sequence all 3 pulses applied are 90° pulses. As in PRESS, they are all simultaneous with different field gradients. After time TE1/2 from the first pulse, a second 90° pulse is applied. The time elapsed between the second and the third pulse is conventionally called mixing time (MT), and is shorter than TE. The signal is finally achieved after time TE + MT from the first pulse (see **Fig. 2**). Thus, the total time for the STEAM technique is shorter than that for PRESS. Spoiler gradients are also needed to reduce signal from regions outside the VOI.

The STEAM sequence uses only 90° pulses, which results in 50% lower SNR than for PRESS. As described, the PRESS sequence is acquired using 2 pulses of 180°. The use of these 180° pulses results in a less optimal VOI profile and leads to a higher SNR. However, because the length of 180° pulses is longer than 90°, PRESS cannot be achieved with a very short TE. Another disadvantage of the PRESS sequence is the larger chemical-shift displacement artifact, which is described later in this article. Therefore, STEAM is usually the modality of choice when a short TE and precise volume selection is needed. Nevertheless, PRESS is the most used SVS technique because it doubles the SNR, which is an important factor that leads to better spectral quality.

Magnetic resonance spectroscopy imaging

MR spectroscopy imaging, also called spectroscopic imaging or chemical-shift imaging, is a multivoxel technique. The main objective of MR spectroscopy imaging is to simultaneously acquire many voxels and a spatial distribution of the metabolites within a single sequence. Thus, this ^{1}H-MRS technique uses phase-encoding gradients to encode spatial information after the RF pulses and the gradient of slice selection.

MR spectroscopy imaging is acquired using only slice selection and phase-encoding gradients, besides the spoiler gradients. A frequency encoding gradient is not applied. Thus, instead of the anatomic information given by the conventional MR imaging signal, the ^{1}H-MRS signal results in a spectrum of metabolites with different frequencies (information acquired from chemical-shift properties of each metabolite).

The same sequences used for SVS are used for the signal acquisition in MR spectroscopy imaging (STEAM or PRESS). The main difference between MR spectroscopy imaging and SVS is that, after the RF pulse, phase-encoding gradients are used in 1, 2, or 3 dimensions (1D, 2D, or 3D) to sample the *k*-space (**Fig. 3**). In a 1D sequence the phase encoding has a single direction, in 2D it has 2 orthogonal directions, and in 3D it has 3 orthogonal directions.

The result of a 2D MR spectroscopy imaging is a matrix, called a spectroscopy grid. The size of this grid corresponds to the field of view (FOV) previously determined. In the 3D sequence, many grids are acquired within one FOV. The number of partitions (or voxels) of the grids is directly proportional to the number of phase-encoding steps. The spatial resolution is also proportional to the number of voxels in

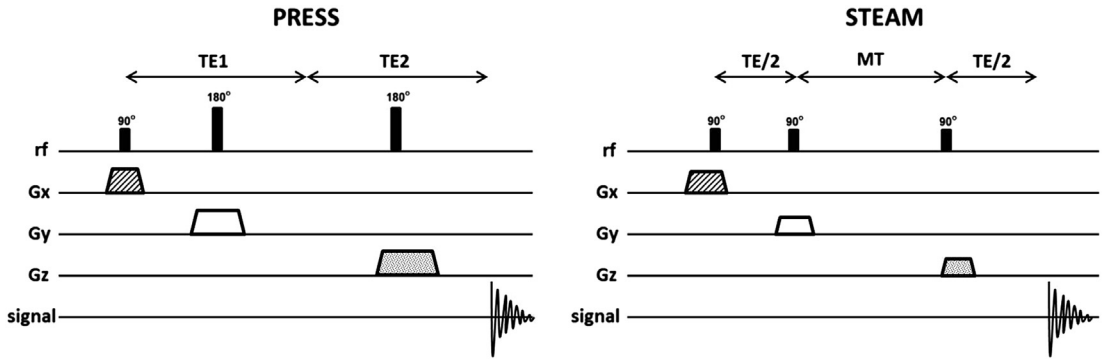

Fig. 2. Schemes of PRESS and STEAM sequences. To simplify, only slice selection gradients are shown. Gz, Gy, and Gx, orthogonal planes; MT, mixing time; rf, radiofrequency pulses; TE, echo time.

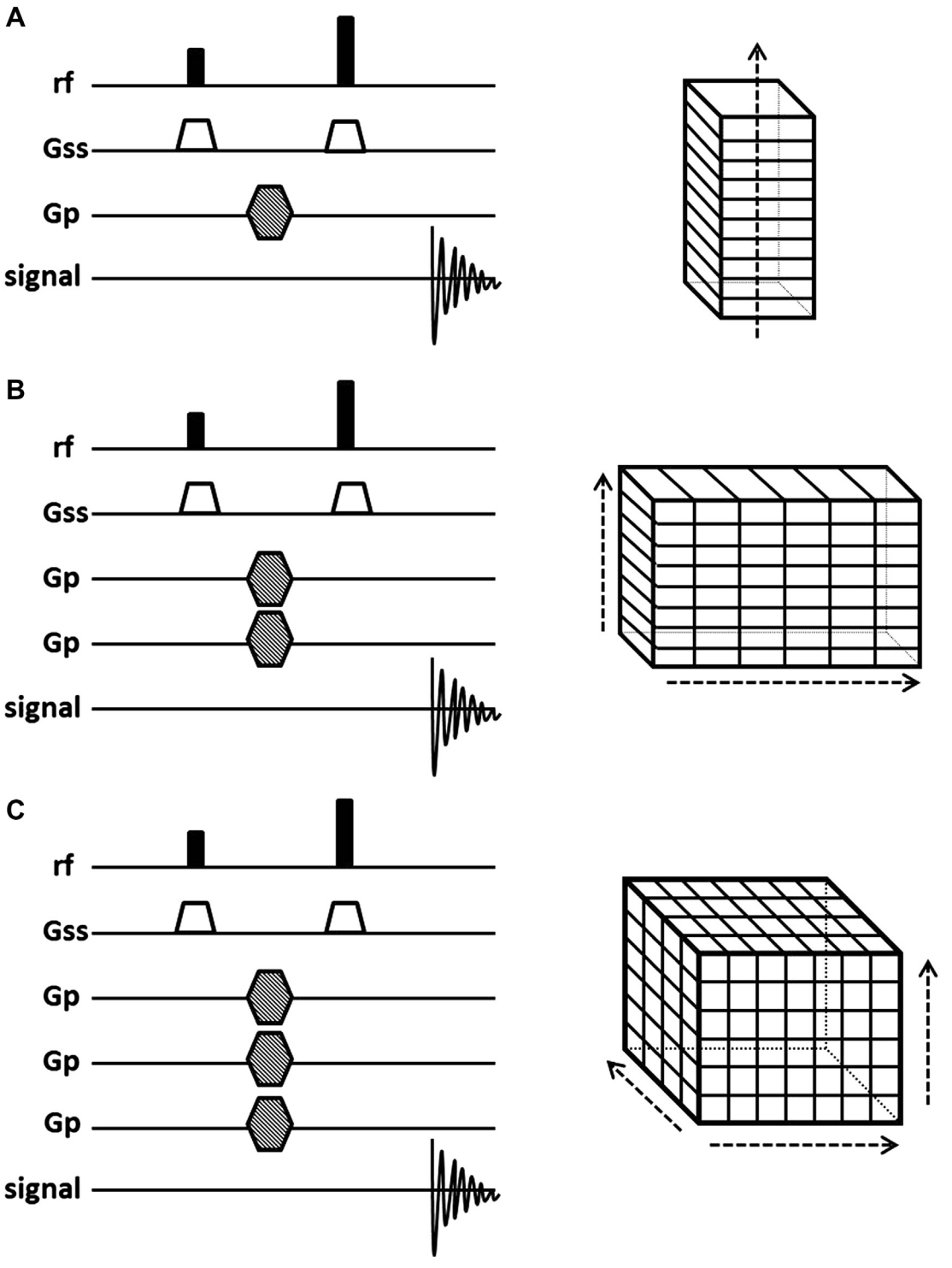

Fig. 3. Scheme of 1-dimensional (*A*), 2-dimensional (*B*), and 3-dimensional MR spectroscopy imaging (*C*) with the localization of columns, slices, and voxels. Gp, phase-encoding gradient; Gss, slice-selection gradient; rf, radiofrequency pulses.

a determined FOV (more voxels give a better spatial resolution). However, for a larger number of voxels, more phase-encoding steps are needed, and this implies a longer time for acquisition. Spatial resolution is also determined by the size of the FOV (a smaller FOV gives better spatial resolution) and by the point-of-spread function (PSF).

PSF on an optical system is defined as the distribution of light from a single point source. For MR spectroscopy imaging, the PSF is related to voxel contamination with signals from adjacent voxels, also called voxel "bleeding." This same effect corresponds to the Gibbs ringing artifact seen on conventional MR imaging. The shape of PSF is determined by the *k*-space sampling method and the number of phase-encoding steps. PSF can be avoided when more than 64 phase-encoding steps are applied, which leads to a scanning time not feasible in clinical practice. To reduce PSF, methods such as *k*-space filtering and reduction are used. For *k*-space reduction, the measured data are restricted to a circular (2D) or spherical (3D) region.

Another concern about MR spectroscopy imaging is the suppression of unwanted signals from outside the brain, particularly from the subcutaneous fat, because lipids have a much higher signal than brain metabolites. Because the FOV is always rectangular and does not conform to the shape of the brain, some techniques must be implemented to optimize the FOV. The use of outer-volume suppression (OVS) is the technique most used for this purpose.

All techniques that help optimize the MR spectroscopy imaging sequence by reducing voxel bleeding, and by increasing spatial resolution and the amount of phase encoding needed to acquire a 2D or 3D MR spectroscopy image, have a time cost. Therefore to minimize scan time without reducing quality, fast MR spectroscopy imaging techniques are used. A large FOV means a longer MR spectrum acquisition time. A simple way to reduce time is to use the smallest possible FOV consistent with the dimension of the object to be analyzed.

Reducing the *k*-space sampling by measuring the data inside a circular or spherical region instead of a rectangular one is another way to reduce scan time. Other techniques used for this purpose are turbo-MR spectroscopy imaging (using multiple spin echoes), multislice MR spectroscopy imaging, 3D echo-planar spectroscopic imaging, and parallel imaging methods. These techniques are beyond the scope of this article, and more details on these methods can be found elsewhere.[1–3]

SVS versus MR spectroscopy imaging

SVS and MR spectroscopy imaging have advantages and disadvantages, depending on the specific purpose (**Table 1**). The SVS technique results in a high-quality spectrum, short scan time, and good field homogeneity. Thus, SVS technique is usually obtained with short TE because longer TE has a decreased signal owing to T2 relaxation. SVS is used to obtain an accurate quantification of the metabolites.

The main advantage of MR spectroscopy imaging is spatial distribution, compared with SVS that only acquires the spectrum in a limited brain region. Moreover, the grid obtained with MR spectroscopy imaging allows voxels to be repositioned during postprocessing. On the other hand, the quantification of the metabolites is not as precise when using MR spectroscopy imaging because of voxel bleeding. Therefore, MR spectroscopy imaging can be used to determine spatial heterogeneity.

Short TE versus long TE

^{1}H-MRS can be obtained using different TEs that result in distinct spectra. Short-TE studies (typically 20–40 milliseconds) have a high SNR and less signal loss because of T2 and T1 weighting. These short-TE properties result in a spectrum with more metabolites peaks, such as myoinositol and glutamine-glutamate (**Fig. 4**), which are not detected with long TE. Nevertheless, because more peaks are shown on the spectrum, overlap is much more common, and care must be taken when quantifying the peaks of metabolites.

^{1}H-MRS spectra may also be obtained with long TEs, from 135 to 288 milliseconds. Long TEs have a poorer SNR; however, they have more simple spectra because of the suppression of some signals. Thus, the spectra are less noisy but have a limited number of sharp resonances. On 135- to 144-millisecond TEs, the peak of lactate is

Table 1
Differences between single-voxel spectroscopy (SVS) and MR spectroscopy imaging

SVS	MR Spectroscopy Imaging
Short TE	Long TE
One voxel	Multivoxel
Limited region	Many data collected
Fixed grid	Grid may be shifted after acquisition
More accurate	Voxel bleeding
Quantitative measurement	Spatial distribution

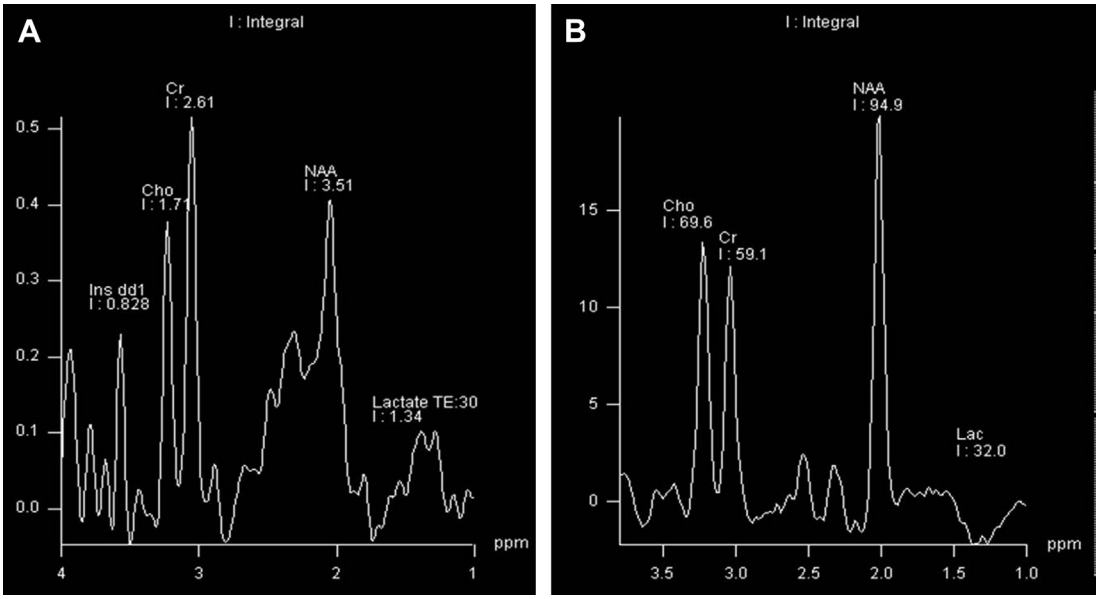

Fig. 4. Spectrum obtained with echo time (TE) = 30 milliseconds (*A*) and TE = 135 milliseconds (*B*). Note the inverted lactate peak (doublet) with long TE acquisition and the increased number of sharp resonances with short TE. Cho, choline; Cr, creatine; Ins dd1, myoinositol; NAA, *N*-acetylaspartate.

inverted below the baseline. This factor is important because the peaks of lactate and lipids overlap in this spectrum. Therefore, 135- to 144-millisecond TEs allow for easier recognition of the lactate peak (see **Fig. 4**) because lipids remain above the baseline. With a TE of 270 to 288 milliseconds there is a lower SNR and the lactate peak is not inverted.

Water Suppression

^{1}H-MRS–visible brain metabolites have a low concentration in brain tissues. Water is the most abundant, and thus its signal in the ^{1}H-MRS spectrum is much higher than that of other metabolites (the signal of water is 100,000 times greater than that of other metabolites). To avoid this high peak from water to be superimposed on the signal of other brain metabolites, water-suppression techniques are needed (**Fig. 5**). The most commonly used technique is chemical-shift selective water suppression (CHESS), which presaturates the water signal using frequency-selective 90° pulses before the localizing pulse sequence. Other techniques sometimes used are variable pulse power and optimized relaxation delays (VAPOR) and water suppression enhanced through T1 effects (WET).

Postprocessing

Quantification and analysis methods of collected data are as important as the acquisition techniques used to obtain the spectra. Using an incorrect postprocessing method may lead to wrong interpretations. There are many postprocessing techniques that may be used before and after the Fourier transform (FT).

The properties of the spectrum can be manipulated using digital filters before the FT. Zero-filling, multiplication with a filter, eddy-current correction, and band-reject filters are some examples of postprocessing steps in the time domain. The use of zero-filling results in a higher digital resolution in the spectrum. Band-reject filters are used to remove residual water signal when the water-suppression technique used during signal acquisition does not completely eliminate it. Eddy-current correction is used to eliminate eddy-current artifacts (explained in the Artifacts section) using a reference signal such as unsuppressed water signal and applying a time-dependent phase correction. After the FT, in the frequency domain, phase and baseline correction are usually used. All these postprocessing methods may be used with SVS and MR spectroscopy imaging. However, because MR spectroscopy imaging uses phase-encoding gradients, other filters need to be applied before FT (eg, Hanning, Hamming, and Fermi filters).

Artifacts

^{1}H-MRS is prone to artifacts. Motion, poor water or lipid suppression, field inhomogeneity, eddy

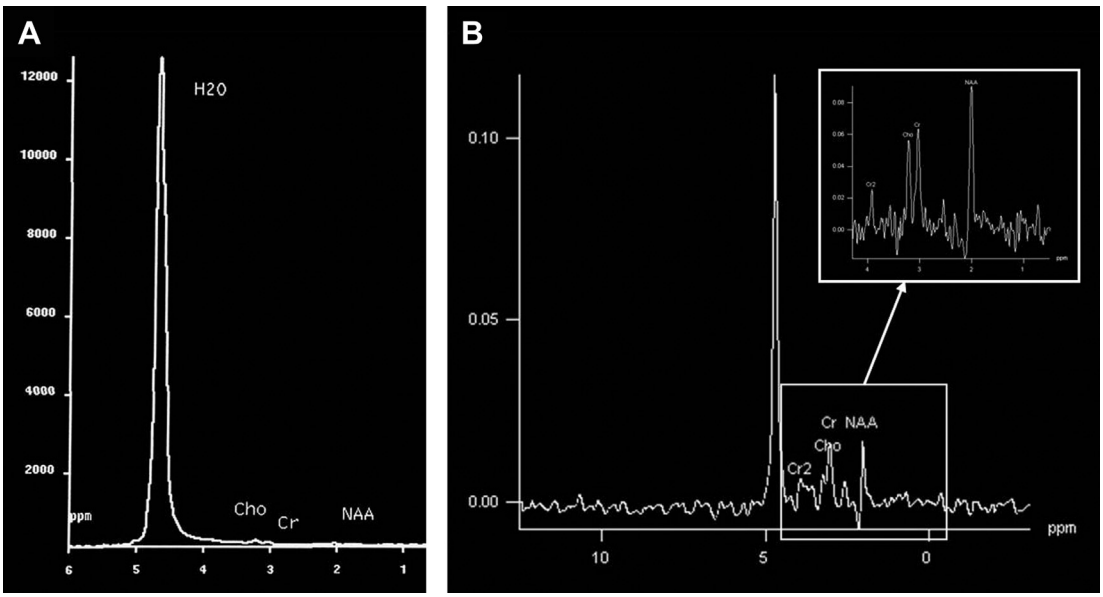

Fig. 5. Water-signal suppression with chemical-shift selective water suppression (CHESS). Spectrum before CHESS (*A*) and after CHESS (*B*). CHESS reduces the signal from water by a factor of 1000, allowing brain metabolites to be depicted on the spectrum. Cho, choline; Cr and Cr2, creatine; NAA, *N*-acetylaspartate.

currents, and chemical-shift displacement are some examples of factors that introduce artifacts into spectra. One of the most important factors that predict the quality of a spectrum is the homogeneity of the magnetic field. Poor field homogeneity results in a lower SNR and broadening of the width of the peaks. For brain ^{1}H-MRS, some regions are more susceptible to this artifact, including those near bone structures and air-tissue interfaces. Therefore, placement of the VOI near areas such as inferior and anterior temporal cortices and orbitofrontal regions should be avoided. Paramagnetic devices also result in field inhomogeneity, leading to a poor-quality spectrum when the VOI is placed near them.

Eddy currents are caused by gradient switching. A transient current results in distortion of the peak shapes, making spectrum quantification difficult. This artifact is more commonly seen in older MR imaging units. However, even modern units produce smaller eddy-current artifacts, and eddy-current correction (used postprocessing) is needed.

Chemical-shift displacements correspond to chemical-shift artifacts on conventional MR imaging. The localization of the voxel is based on the precession frequency of the protons. Because this frequency is different for each metabolite, the exact position of each metabolite is slightly different. This artifact is larger with higher magnetic field strengths. To solve this problem, strong field gradients must be used for the slice selection.

Higher-Field ^{1}H-MRS

Higher-field MR imaging (3 T, 7 T, and above) is used in many centers mostly for research purposes. In the past decade 3-T MR imaging has started to be routinely used for clinical examinations, resulting in better SNR and faster acquisition time.

^{1}H-MRS at 3 T has a higher SNR and shorter acquisition time than when performed at 1.5 T. It had been assumed that SNR increases linearly with the strength of the magnetic field, but SNR does not double with 3-T ^{1}H-MRS because others factors are also responsible for the SNR, including metabolite relaxation time and magnetic-field homogeneity.

Spectral resolution is improved with a higher magnetic field. A better spatial resolution increases the distance between peaks, making it easier to distinguish between them. This aspect is important, particularly for resonances from coupled spins such as glutamate, glutamine, and myoinositol. However, the line-width of metabolites also increases at higher magnetic field because of a markedly increased T2 relaxation time. Thus, a short TE is more commonly used with 3 T. The difference in T1 relaxation time from 1.5 to 3 T depends on the brain region studied.[4]

3-T ^{1}H-MRS is more sensitive to magnetic-field inhomogeneity, and some artifacts are more pronounced (eg, susceptibility and eddy currents). Chemical-shift displacement is also greater at 3 T,

and this artifact increases linearly with the magnetic field.

Receiver coils have also improved. The use of multiple RF receiver coils for ^{1}H-MRS provides higher local sensitivity and results in a higher SNR. These coils also allow a more extended coverage of the brain.

SPECTRA

^{1}H-MRS allows the detection of brain metabolites. The metabolite changes often precede structural abnormalities, and ^{1}H-MRS can demonstrate abnormalities before MR imaging does.[5] To detect these spectral alterations, it is fundamental to know the normal brain spectra and their variations according to the applied technique, patient's age, and brain region.

^{1}H spectra of metabolites are shown on x and y axes. The x (horizontal) axis displays the chemical shift of the metabolites in units of ppm. The ppm increases from right to left. The y (vertical) axis demonstrates arbitrary signal amplitude of the metabolites. The height of metabolic peak refers to a relative concentration, and the area under the curve to metabolite concentration.[5]

Long TE sequences result in less noise than short TE sequences, but several metabolites are better demonstrated with short TE. In 1.5-T MR scanners, long TE sequences (TE = 135–288 milliseconds) detect *N*-acetylaspartate (NAA), creatine (Cr), choline (Cho), lactate (Lac) and, possibly, alanine (Ala). Short TE sequences (TE = 20–40 milliseconds) demonstrate the metabolites seen with long-TE acquisitions and, in addition, lipids, myoinositol (Myo), glutamate-glutamine (Glx), glucose, and some macromolecular proteins (Fig. 6).

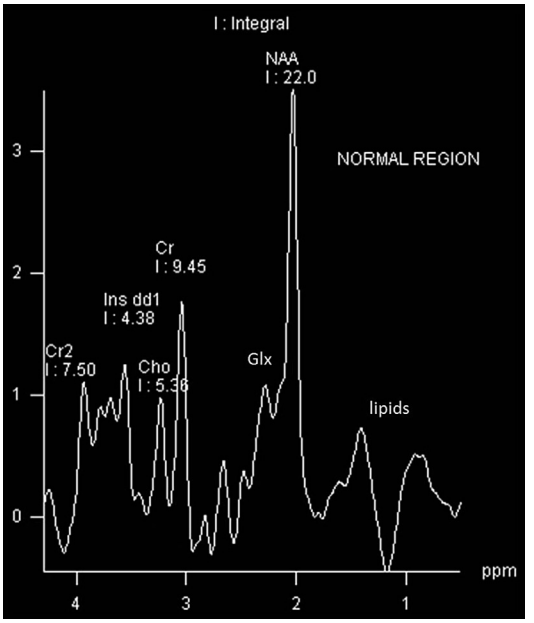

Fig. 6. Normal spectra obtained with short TE sequence. (TE = 30 milliseconds). Cho, choline; Cr, and Cr2, creatine; Glx, glutamate-glutamine; Ins dd1, myoinositol; NAA, *N*-acetylaspartate.

Brain Metabolites

N-acetylaspartate

The peak of NAA is the highest peak in normal brain, assigned at 2.02 ppm. NAA is synthesized in the mitochondria of neurons, then transported into neuronal cytoplasm and along axons. NAA is exclusively found in the nervous system (peripheral and central), and is detected in both gray and white matter. It is a marker of neuronal and axonal viability and density. NAA can additionally be found in immature oligodendrocytes and astrocyte progenitor cells. NAA also plays a role as a cerebral osmolyte.

Absence or decreased concentration of NAA is a sign of neuronal loss or degradation. Neuronal destruction from malignant neoplasms and many white-matter diseases results in decreased concentration of NAA. By contrast, increased NAA indicates Canavan disease, although it may also be demonstrated in Salla disease and Pelizaeus-Merzbacher disease. NAA is not demonstrated in extra-axial lesions such as meningiomas or intra-axial ones originating from outside of the brain such as metastases, unless there is a partial volume effect with normal parenchyma.

Creatine

The peak of the Cr spectrum is assigned at 3.02 ppm. This peak represents a combination of molecules containing creatine and phosphocreatine. Cr is a marker of energetic systems and intracellular metabolism. The concentration of Cr is relatively constant, and it is considered a stable metabolite. It is therefore used as an internal reference for calculating metabolite ratios. However, there is regional and individual variability in Cr concentrations.

In brain tumors, the Cr signal is relatively variable (see later discussion). Gliosis may cause minimally increased Cr, owing to increased density of glial cells (glial proliferation). Creatine and phosphocreatine are metabolized to creatinine, then the creatinine is excreted via the kidneys.[6] Systemic disease (eg, renal disease) may also affect Cr levels in the brain.[7]

Choline

The Cho spectrum peak is assigned at 3.22 ppm and represents the sum of choline and choline-containing compounds (eg, phosphocholine). Cho is a marker of cellular membrane turnover

(phospholipids synthesis and degradation) reflecting cellular proliferation. In tumors, Cho levels correlate with degree of malignancy reflecting cellularity. Increased Cho may be seen in infarction (from gliosis or ischemic damage to myelin) or inflammation (glial proliferation). For this reason, Cho is considered to be nonspecific.

Lactate

The Lac peak is difficult to visualize in the normal brain. The peak of Lac is a doublet at 1.33 ppm, which projects above the baseline on short/long TE acquisition and inverts below the baseline at TE of 135 to 144 milliseconds.

A small peak of Lac is visible in some physiologic states such as newborn brains during the first hours of life.[8] Lac is a product of anaerobic glycolysis, so its concentration increases under anaerobic metabolism such as cerebral hypoxia, ischemia, seizures, and metabolic disorders (especially mitochondrial ones). Increased Lac signals also occur with macrophage accumulation (eg, acute inflammation). Lac also accumulates in tissues with poor washout such as cysts, normal-pressure hydrocephalus, and necrotic and cystic tumors.[7]

Lipids

Lipids are components of cell membranes not visualized with long TE because of their very short relaxation time. There are 2 peaks of lipids: methylene protons at 1.3 ppm and methyl protons at 0.9 ppm.[9] These peaks are absent in the normal brain, but presence of lipids may result from improper voxel selection, causing voxel contamination from adjacent fatty tissues (eg, fat in subcutaneous tissue, scalp, and diploic space).

Lipid peaks can be seen when there is cellular membrane breakdown or necrosis, such as in metastases or primary malignant tumors.

Myoinositol

Myo is a simple sugar assigned at 3.56 ppm. Myo is considered a glial marker because it is primarily synthesized in glial cells, almost only in astrocytes. It is also the most important osmolyte in astrocytes. Myo may represent a product of myelin degradation. Elevated Myo occurs with proliferation of glial cells or with increased glial-cell size, as found in inflammation. Myo is elevated in gliosis, astrocytosis, and Alzheimer disease (AD).[7,9]

Alanine

Ala is an amino acid that has a doublet centered at 1.48 ppm. This peak is located above the baseline in spectra obtained with short/long TE and inverts below the baseline on acquisition using TE of 135 to 144 milliseconds. Its peak may be obscured by Lac (at 1.33 ppm). The function of Ala is uncertain, but it plays a role in the citric acid cycle.[7] Increased concentration of Ala may occur in defects of oxidative metabolism.[9] In tumors, an elevated level of Ala is specific for meningiomas (**Fig. 7**).

Glutamate-glutamine

Glx has complex peaks from glutamate, glutamine, and γ-aminobutyric acid assigned at 2.05 to 2.50 ppm. These metabolite peaks are difficult to separate at 1.5 T. Glutamate is an important excitatory neurotransmitter and also plays a role in the redox cycle.[7,9] Elevated concentration of glutamine are found in a few diseases such as hepatic encephalopathy.[5,9]

Regional Variations of the Spectra

Metabolite peaks may differ slightly according to the brain region being studied. Studies have shown differences between the spectra of white and gray matter and between supratentorial and infratentorial structures. Nevertheless, no significant asymmetries of metabolite spectra between the left and right hemispheres or between genders have been found.[10,11]

In specific quantitative techniques, the concentration of NAA in gray matter is higher than that in white matter. For clinical purposes, concentrations of NAA in both gray and white matter are not significantly different. Most studies have found higher Cho levels in white matter than in gray matter, whereas the Cr level is higher in gray matter.[6,12–14] There are some frontal-occipital variations too. The clearest difference is a caudal decrease in Cho in the cortex.[15,16] Regional variations of Glx and Myo have been studied less than those of NAA, Cho, and Cr. One study[17] found higher Glx levels in gray matter than in white matter. The regional distribution of Myo is unclear, but tends to be higher in gray matter than in white matter.[17]

Regarding the brainstem and cerebellum, the highest levels of NAA are in the pons.[18] Significantly higher levels of Cho have been found in the cerebellum and pons than in supratentorial regions.[16,18] Cerebellar levels of Cr are also significantly higher than supratentorial levels, whereas low levels of Cr are seen in the pons.[16,18]

^{1}H-MRS of the hippocampus has been studied especially in epilepsy and AD. There are anterior-posterior gradients of metabolites in the hippocampi. The concentration of Cho increases from the posterior to anterior hippocampus, whereas a lower NAA concentration has been found anteriorly.[19,20]

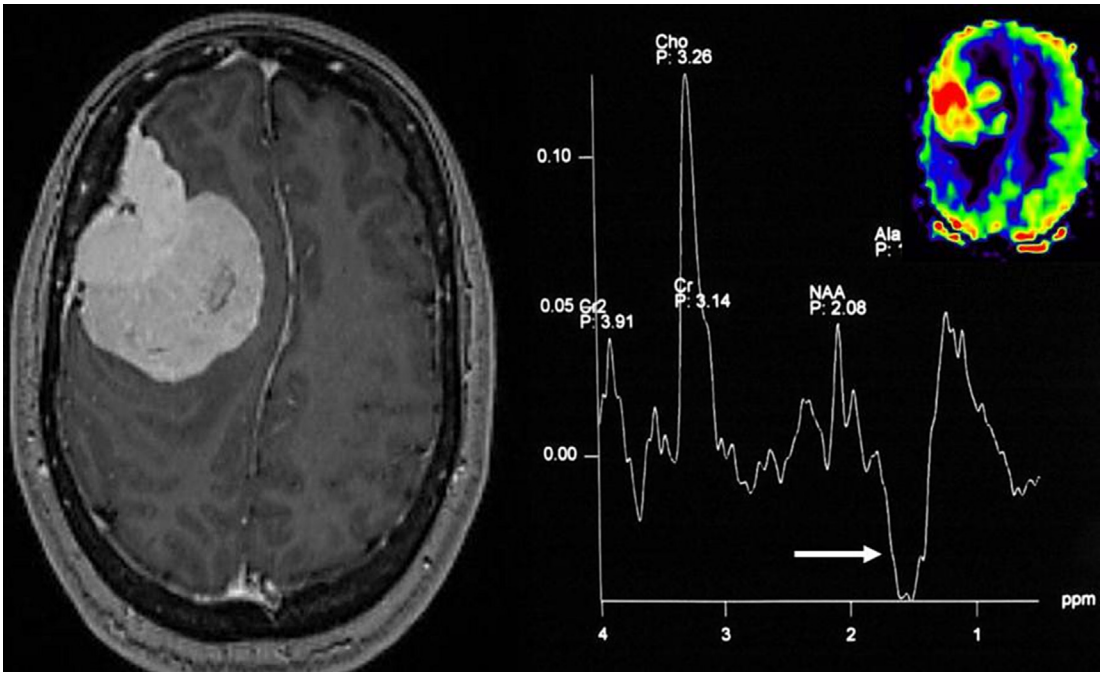

Fig. 7. Extra-axial mass on the right frontal region with enhancement post gadolinium on T1-weighted imaging and hyperperfusion on arterial spin-labeling volume map (*upper right*). An inverted doublet peak is seen at 1.48 ppm at ^{1}H-MRS that corresponds to alanine (*arrow*). High peaks of Cho and low NAA are also depicted. Ala, alanine; Cho, choline; Cr and Cr2, creatine; NAA, *N*-acetylaspartate.

Spectra in Pediatrics

Regardless of the differences in methodology, there are differences in metabolite levels in the developing brain. MR spectra depend on age, and during the first year of life significant changes occur. In general, the spectral pattern in pediatrics is considered to be similar to that of adults when older than 2 years of age, and the concentration of metabolites is practically constant by 4 years of age.[7,21,22] NAA levels are low, whereas levels of Myo and Cho are high at birth. Both gray and white matter show similar patterns. Myo is a prominent metabolite in brain spectra of newborns. As age increases, increased concentration of NAA and decreased concentrations of choline-containing compounds and Myo become evident.[5,7,21] Concentrations of Cr and phosphocreatine are constant and may be used as reference values (**Fig. 8**). An increased concentration of NAA reflects brain maturation, and its concentration correlates with myelination.[6,21] With cerebral maturation, there is also a decrease in the concentration of Cho compounds. A small amount of Lac may be seen in newborn brains.[8] Glutamate and glutamine do not demonstrate significant alterations with age.[21]

According to gestational age, the equation of Kreis and colleagues[22] describes changes in metabolite concentration. With this equation and parameters for a multiexponential model,[21] graphs of metabolite changes with age can be drawn (**Fig. 9**).

Spectra in the Elderly

^{1}H-MRS studies of elderly brains are less consistent than those of pediatric brains. Some studies have found a reduced concentration of NAA with aging, which suggests a decrease in neuronal mass.[7,23,24] By contrast, other studies have found relatively stable concentrations of NAA in older groups but increased Cho and/or Cr.[14,25] A systematic review of ^{1}H-MRS in healthy aging summarized the findings of ^{1}H-MRS in aging in that they are varied. Most studies have reported no changes in metabolites with advanced age. However, some data suggest lower NAA and higher Cho and Cr with increasing age.[26] Disagreement of the studies could be due to the use of different techniques (eg, evaluation of different brain regions and atrophy correction). Different study populations may also affect results.

CLINICAL APPLICATION

Brain Tumors

Brain tumors are currently the main application of ^{1}H-MRS. This technique is usually used as

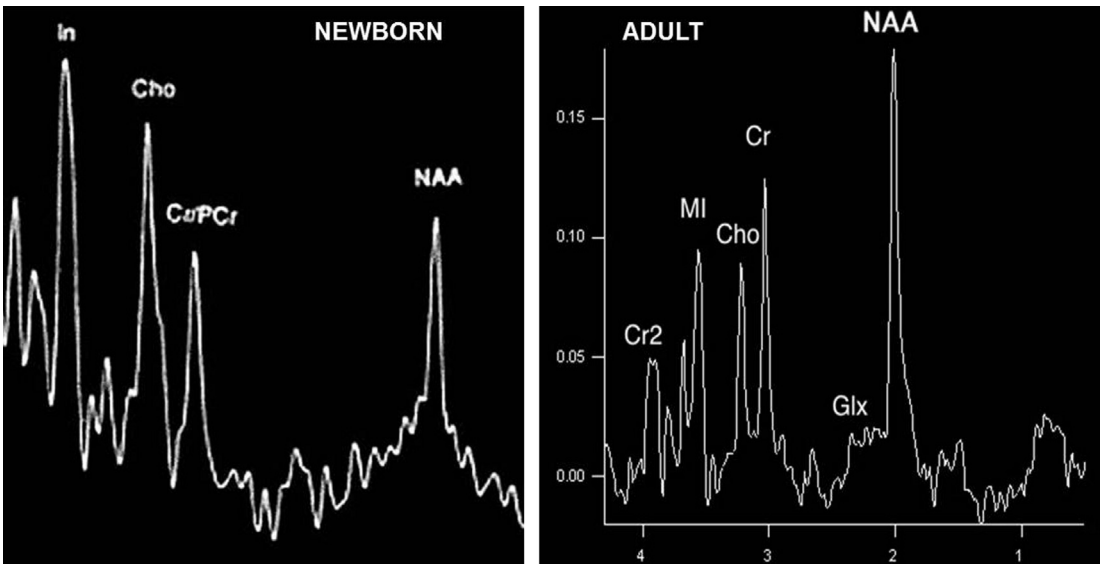

Fig. 8. Normal spectra in newborn (*left*) demonstrate high levels of myoinositol (Myo) and Cho but low NAA compared with the normal spectra in an adult (*right*). Cho, choline; CrPcr, creatine/phosphocreatine; Cr and Cr2, creatine; Glx, glutamate-glutamine; In, Myo; MI, Myo; NAA, *N*-acetylaspartate.

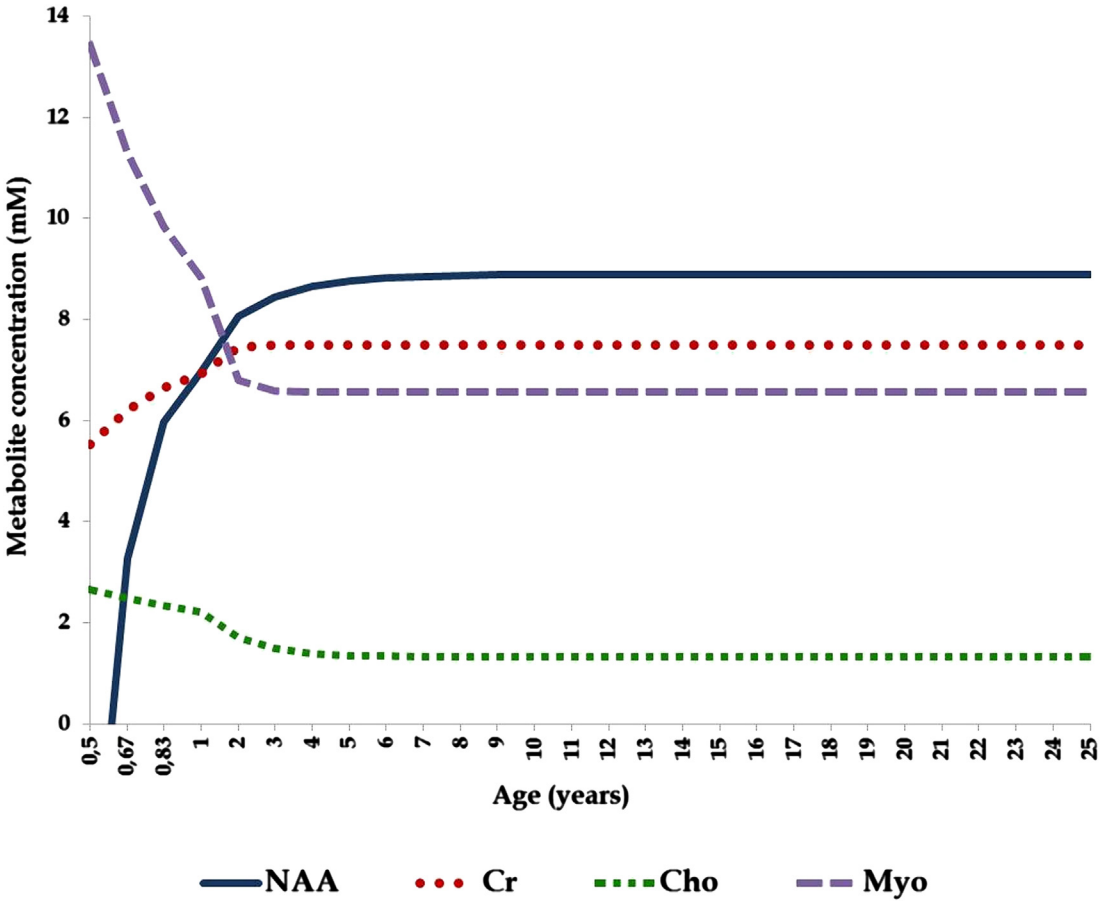

Fig. 9. Changes in metabolite concentrations with age calculated by the equation of Kries and colleagues and the parameters of Dezortova and Hajek. Cho, choline; Cr, creatine; Myo, myoinositol; NAA, *N*-acetylaspartate.

a complement to conventional MR imaging, along with other advanced techniques such as perfusion. Combined with conventional MR imaging, proton MR spectra may improve diagnosis and treatment of brain tumors. ^{1}H-MRS may help with differential diagnosis, histologic grading, degree of infiltration, tumor recurrence, and response to treatment, mainly when radionecrosis develops, and is indistinguishable from tumor by conventional MR imaging.

An important decision regarding analysis of intracranial masses concerns which ^{1}H-MRS technique to use. Different ^{1}H-MRS parameters may be varied to optimize the results, the most relevant of which is TE.[27] Short TE allows for recognition of more peaks than does long TE, which may be important for the differential diagnosis of brain masses and for grading tumors. Myo is a marker for low-grade gliomas, only seen on short-TE acquisitions. However, longer TEs give a spectrum with a limited number of peaks, making it easier to analyze. Long TEs varying from 135 to 140 milliseconds also invert peaks of Lac and Ala. This inversion is important for differentiating between these peaks and lipids, because they commonly overlap. Hence, the choice of TE may be difficult, and one solution is to acquire 2 different spectra using both short and long TEs. In clinical practice, 2 ^{1}H-MRS acquisitions are rarely feasible because of time constraints.

MR spectroscopy imaging is usually preferable to SVS because of its spatial distribution. It allows the acquisition of a spectrum of a lesion and the adjacent tissues, and also gives a better depiction of tumor heterogeneity. However, MR spectroscopy imaging is generally combined with long TE instead of short TE. SVS, on the other hand, is faster and can be obtained using both long and short TEs. When using SVS, the VOI should be placed within the mass, avoiding contamination from adjacent tissues. An identical VOI must be positioned on the homologous region of the contralateral hemisphere for comparison, whenever possible.

Elevation of Cho is seen in most neoplastic lesions. The Cho peak may help with treatment response, diagnosis, and progression of tumor. Its increase has been attributed to cellular membrane turnover, which reflects cellular proliferation. One prospective study[28] analyzing 18 gliomas showed that the Cho signal correlated linearly with cell density (inversely to what is seen with the apparent diffusion coefficient) instead of the proliferative index. The Cho peak is usually higher in the center of a solid neoplastic mass, and decreases peripherally. The Cho signal is consistently low in necrotic areas.

Another ^{1}H-MRS feature seen in brain tumors is decreased NAA. This metabolite is a neuronal marker, and its reduction denotes destruction and displacement of normal tissue. Absence of NAA in an intra-axial tumor generally implies an origin outside of the central nervous system (metastasis) or a highly malignant tumor that has destroyed all neurons in that location. The Cr signal, on the other hand, is slightly variable in brain tumors, and changes according to tumor type and grade. The typical ^{1}H-MRS spectrum for a brain tumor is one of a high level of Cho, low NAA, and minor changes in Cr (**Fig. 10**).

Cho elevation is usually evidenced by an increase in Cho/NAA or Cho/Cr ratios, rather than its absolute concentration. Estimation of absolute Cho concentration, although possible, is susceptible to many errors because many assumptions are required. Therefore, Cho/NAA and Cho/Cr ratios are accurate for establishing Cho levels in brain neoplasms.

When faced with intracranial expansive lesions, conventional MR imaging with or without perfusion may lead to a reliable diagnosis. In doubtful cases, ^{1}H-MRS may play a role in preoperative differential diagnosis (**Table 2**). Studies have shown that the use of ^{1}H-MRS in specific cases improves accuracy and the level of confidence in differentiating neoplastic from nonneoplastic masses.[29] The differentiation of a low-grade glioma from stroke or focal cortical dysplasia (**Fig. 11**) may be difficult or impossible using conventional MR imaging. In these cases, increased levels of Cho make a diagnosis of neoplasm much more likely. In some cases of focal cortical dysplasia, Cho may be moderately increased, probably as a result of intrinsic epileptic ictal activity.[30]

Some expansive lesions may be similar to neoplasms on conventional MR imaging and ^{1}H-MRS. The ^{1}H-MRS spectrum of a giant demyelinating plaque usually shows high Cho and low NAA levels. In the acute stage of a demyelinating disease, increased Lac can also be seen, and may reflect the metabolism of inflammatory cells.[31,32] An increase in Glu[33] and Myo[34] is also noted in multiple sclerosis.

The differential diagnosis between brain abscess and neoplasms (primary and secondary) is another challenge. These features may appear as cystic lesions with rim enhancement on conventional MR imaging. Pyogenic abscesses have high signal intensity on diffusion-weighted imaging, which is usually not seen in tumors. Nevertheless, some neoplasms may occasionally have restricted diffusion, and biopsy is inevitable. In these cases, ^{1}H-MRS may help to establish a diagnosis. If the VOI is positioned in the enhancing area, presence

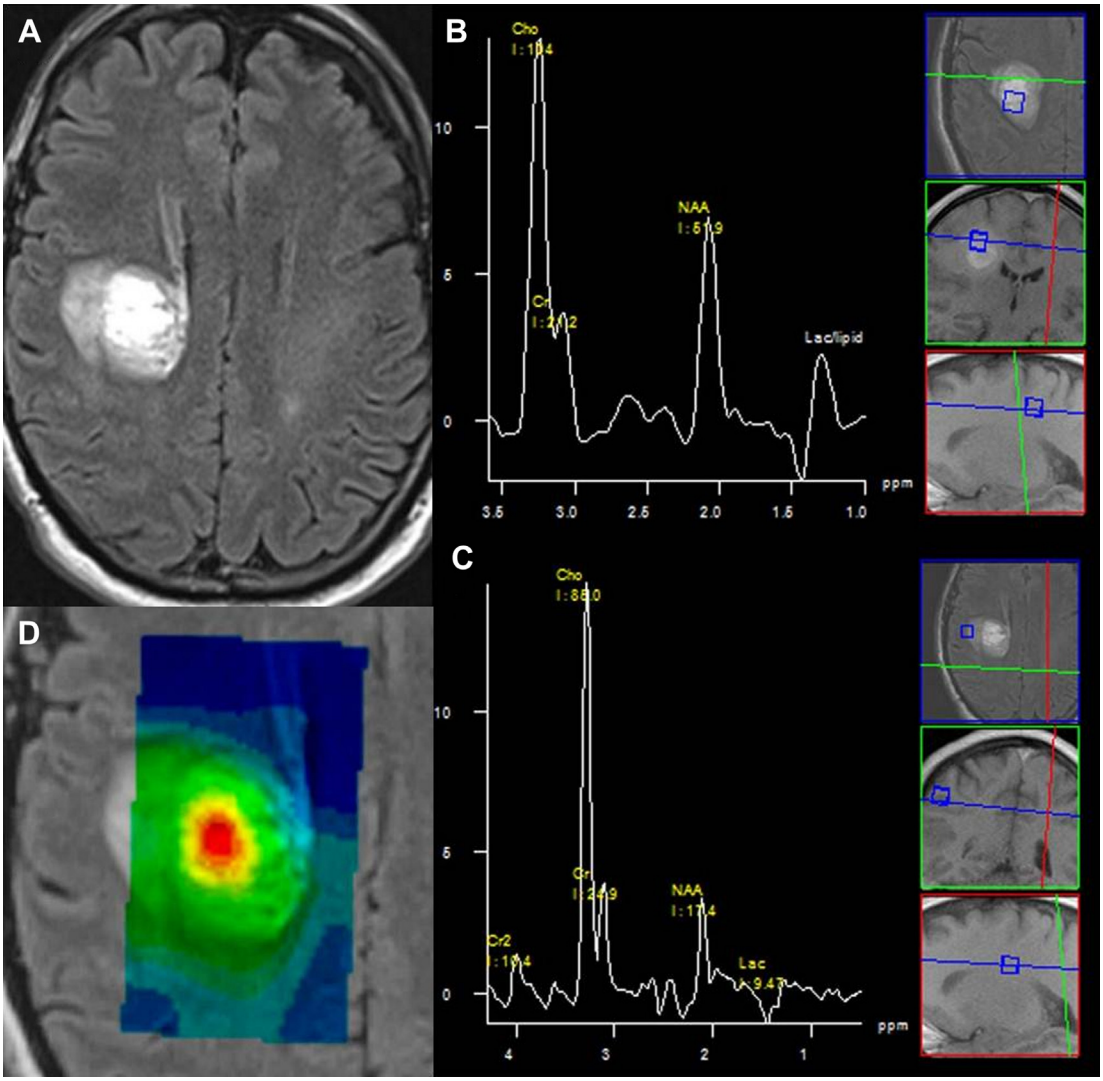

Fig. 10. Histologically confirmed glioblastoma. Axial fluid-attenuated inversion recovery (FLAIR) MR image (*A*) shows a lesion with high signal intensity in a posterior region of the right frontal lobe. ^{1}H-MRS with long TE demonstrates increase in Cho peak and decrease in NAA peak inside the lesion (*B*) and in the surrounding tissue (*C*), representing tumor infiltration. Lactate and lipids are also present. Color metabolite map (*D*) also demonstrates abnormal Cho/Cr ratio. Cho, choline; Cr and Cr2, creatine; Lac, lactate; NAA, *N*-acetylaspartate.

of Cho favors a neoplasm.[35] If the VOI is positioned in the cystic area of a lesion, abscess and tumor both demonstrate a high Lac peak. Nonetheless, the presence of acetate, succinate, and amino acids such as valine, Ala, and leucine in the core of the lesion has high sensitivity for pyogenic abscess (**Fig. 12**).[36,37] These peaks are not seen in tumors. It is important to be aware that in patients with pyogenic brain abscess who are under antibiotic therapy, these peaks may be absent.

^{1}H-MRS can also help in the differentiation of high-grade gliomas from solitary metastasis. Both lesions show the same ^{1}H-MRS pattern, with high Cho and low NAA. However, the high signal intensity on T2-weighted imaging seen in the perilesional area demonstrates an elevated Cho/Cr ratio only in high-grade gliomas (see **Fig. 10**).[38] This feature is consistent with the pathologic findings of infiltrating tumor cells in areas of edema not seen in metastases.

Gliomas, the most common and the most studied lesions among neuroepithelial tumors, originate from glial cells (eg, astrocytes or oligodendrocytes). Gliomas have an infiltrative nature, resulting in neuronal cell damage and decreased NAA. Cohen and colleagues[39] found decreased whole-brain NAA in patients with glial tumors beyond the main tumor. This significant whole-brain NAA depletion

Table 2
^{1}H-MRS changes in tumors and other lesions

	Cho	NAA	Lac	Lip	Myo	Glu	Suc	Acet	Ala	Aa
Low-grade tumor	↑	↓			↑					
High-grade tumor	↑	↓	↑	↑						
Metastasis	↑	Absent[a]	↑	↑						
Oligodendroglioma	↑	↓	↑[b]							
Meningioma	↑	Absent							↑	
Gliomatosis cerebri	↑	↓								
Lymphoma	↑	Absent[a]		↑						
Radionecrosis	↓	↓	↑	↑						
Abscess	N	↓	↑	↑			↑	↑	↑	↑
Demyelination	↑	↓	↑[c]	↑	↑	↑[c]				

Abbreviations: ↑, increased peak; ↓, reduced peak; Aa, amino acids; Acet, acetate; Ala, alanine; Cho, choline; Glu, glutamine; Lac, lactate; Lip, lipids; Myo, myoinositol; N, normal peak; NAA, *N*-acetylaspartate; Suc, succinate.
[a] NAA is absent in the core of the tumor, but may be present where it infiltrates brain parenchyma or with voxel bleeding.
[b] The presence of lactate depends on the grade of the tumor.
[c] Lac and Glu are increased only in the early stage of the disease.

may reflect extensive tumor infiltration in the normal-appearing brain on MR imaging. One quantitative ^{1}H-MRS study[40] found a correlation between the percentage of tumor infiltration from the ^{1}H-MRS–guided biopsy samples and changes in NAA, Cho, and Cho/NAA ratio in corresponding voxels. Absolute concentration of NAA decreased, whereas absolute concentration of Cho and the Cho/NAA ratio increased with degree of tumor infiltration.

Astrocytomas can be classified into low grade (grades I and II, benign) and high grade (grades III and IV, malignant). High-grade gliomas (anaplastic gliomas or grade III, and glioblastoma multiforme or grade IV) have higher Cho and lower NAA than low-grade gliomas. Elevated Cho correlates with cellular proliferation and density. Although several studies in one systematic review[41] have reported that ^{1}H-MRS can accurately differentiate between low-grade and high-grade gliomas, the results of glioma grading using ^{1}H-MRS vary widely. Such wide variations may be attributed to different methods and metabolites overlapping between different tumor grades. Statistically significantly higher Cho/Cr, Cho/NAA, and relative cerebral blood volume (rCBV) have been reported in high-grade in comparison with low-grade gliomas,[42] although threshold values of metabolite ratios for grading of gliomas are not well established. Cho/Cr is the most frequently used ratio. Some institutions use a threshold value of 2.0 for Cho/Cr to differentiate low-grade from high-grade gliomas, whereas some use a cutoff value of 2.5.

As described earlier, lipid and Lac peaks are absent under normal conditions. Lipid peak indicates necrosis in malignant tumors. Lac, a product of anaerobic glucolysis, accumulates in necrotic portions of tumors. The presence of lipids and Lac correlates with necrosis in high-grade gliomas. Compared with high-grade gliomas, low-grade gliomas show higher Myo levels,[43,44] which may be due to a low mitotic index in low-grade gliomas and, thus, fewer mitogens (substances that trigger cell mitosis). Some mitogens can influence the metabolism of phosphatidylinositol, and Myo is also involved in the formation of phosphatidylinositol. Thus, lack of activation of phosphatidylinositol metabolism results in Myo accumulation. Howe and colleagues[44] concluded that high Myo was characteristic of grade II astrocytomas.

On serial ^{1}H-MRS, malignant degeneration of gliomas can be detected using percentage signal change in Cho. Tedeschi and colleagues[45] have demonstrated that interval percentage changes in Cho intensity in stable gliomas and progressive gliomas (malignant degeneration or recurrent disease) is less than 35 and more than 45, respectively. Interval increased Cho/Cr or Cho/NAA is suggestive of malignant progression.

Gliomatosis cerebri is a distinct entity of glial tumors. This rare disease is characterized by diffuse infiltration of glial-cell neoplasm throughout the brain. Gliomatosis cerebri has various histologic subtypes (astrocytoma, oligodendroglioma, or mixed glioma). The World Health Organization (WHO) classification denotes grades II, III, and IV gliomatosis cerebri[46]; therefore, patients with this

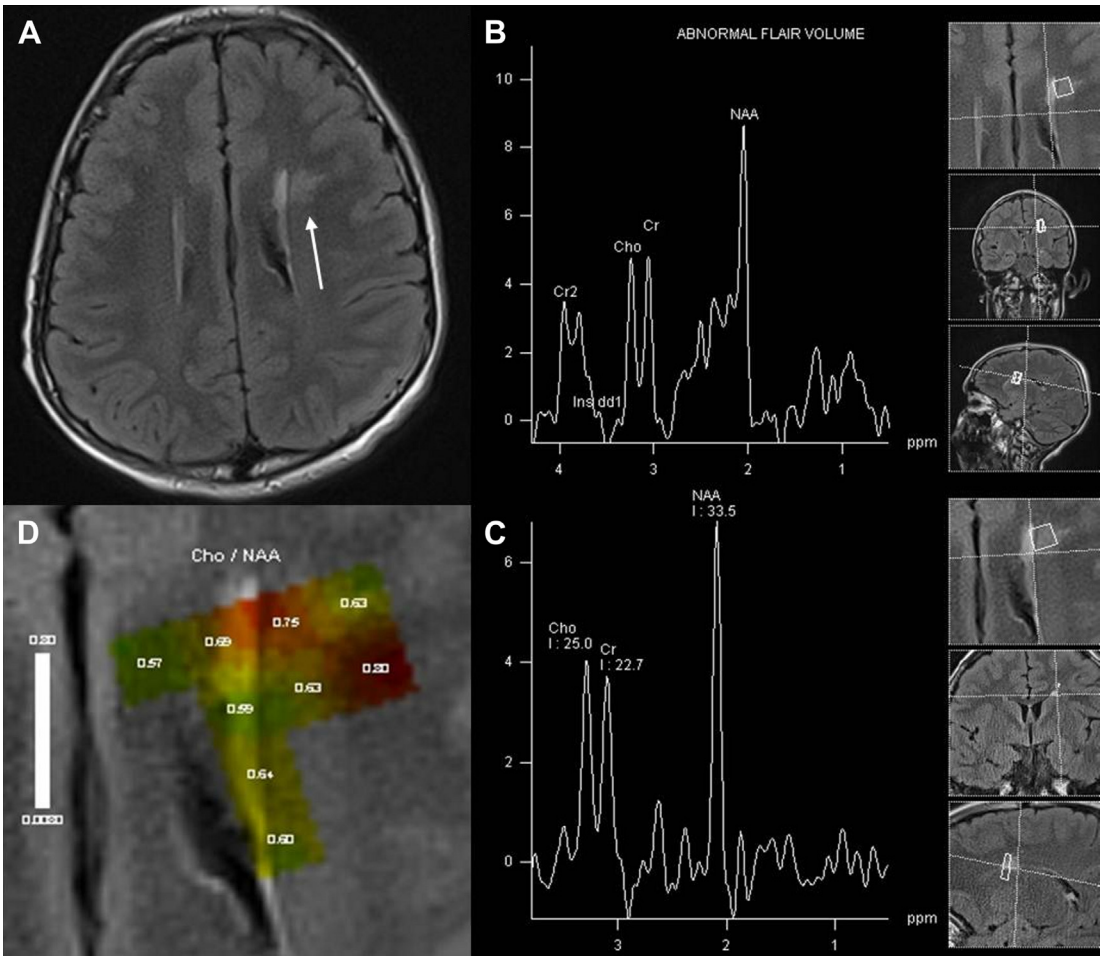

Fig. 11. A 10-year-old boy with intractable seizures. (*A*) FLAIR image shows focal high signal intensity in the white matter of the centrum semiovale of the left frontal lobe (*arrow*) and overlying blurry gray matter–white matter junction. ^{1}H-MRS images with TE = 35 milliseconds (*B*) and TE = 144 (*C*) demonstrate normal Cho and NAA peaks. Color metabolite map (*D*) demonstrates normal Cho/NAA ratio. These findings are suggestive of a cortical dysplasia with adjacent abnormal white matter. Cho, choline; Cr and Cr2, creatine; Ins dd1, myoinositol.

tumor have a widely variable prognosis. Marked elevation of Myo and Cr has been found in gliomatosis cerebri, and this may be attributed to glial activation rather than glial proliferation[47] because the Cho level is moderately elevated, suggesting low density of glial cells.

Oligodendroglioma is a subgroup of gliomas that has a better response to treatment (chemosensitive) and better prognosis than glioblastoma. This distinct tumor is divided into two groups according to the WHO classification: grades II and III.[48] It originates from oligodendrocytes but often contains a mixed population of cells, particularly astrocytes. Loss of genes in chromosomes 1p and 19q is a characteristic genetic alteration of most oligodendrogliomas. On dynamic contrast-enhanced MR perfusion, low-grade oligodendrogliomas may demonstrate high rCBV because they contain a dense network of branching capillaries.[49] Thus several oligodendrogliomas can be misinterpreted as high-grade tumors because of their high rCBV, which contributes to decreasing the reliability of rCBV in differentiating high-grade and low-grade gliomas. Among the low-grade gliomas, low-grade oligodendrogliomas also exhibit significantly higher rCBV on dynamic-contrast MR perfusion.[50] In subgroups of the oligodendroglial tumors, MR imaging studies have found that contrast enhancement is not suggestive of anaplasia as it is in astrocytomas. One study showed that rCBV was not significantly different between low-grade and high-grade oligodendroglimas,[51] in contrast to another study[52] showing rCBV to differ significantly between the low and high grades.

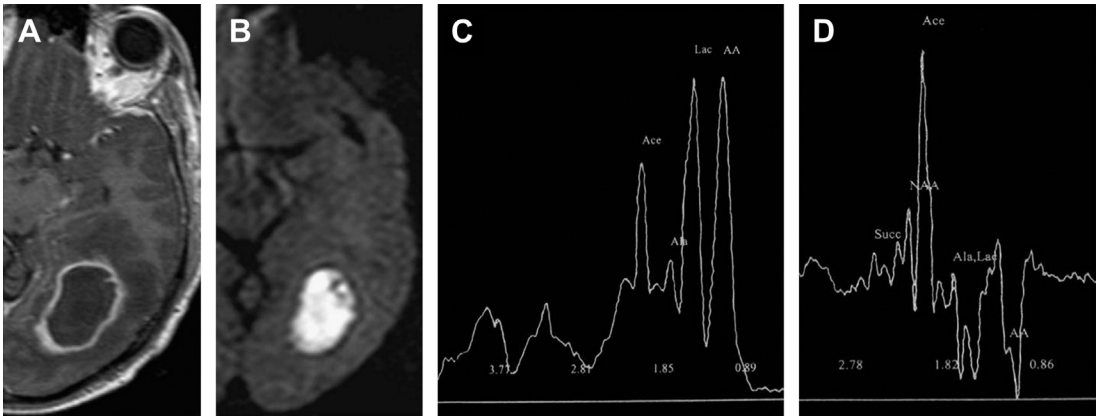

Fig. 12. Parenchymal pyogenic abscess presenting as lesion with rim enhancement after gadolinium injection on T1-weighted imaging (*A*) and high signal diffusion on diffusion-weighted imaging (*B*). ^{1}H-MRS images with short TE (*C*) and long TE (*D*) show high levels of acetate (Ace), alanine (Ala), lactate (Lac), succinate (Succ), and amino acids (AA). The VOI was positioned in the core of the lesion.

The results of ^{1}H-MRS studies in oligodendrogliomas are more consistent than those of MR perfusion studies. Similarly to astrocytomas, ^{1}H-MRS of oligodendrogliomas demonstrates significantly higher Cho, Cho/Cr ratio, and a higher incidence of Lac and lipids in high-grade than in low-grade tumors.[51–53] Nevertheless, low-grade oligodendrogliomas may show highly elevated Cho, mimicking high-grade tumors, because these low-grade tumors can have high cellular density but absent endothelial proliferation and necrosis.[52] Apart from higher rCBV, the level of glutamine plus glutamate is significantly higher in low-grade oligodendrogliomas than in low-grade astrocytomas, and may help to distinguish these tumors from each other.[53]

Accurate grading of gliomas based on ^{1}H-MRS alone may be difficult. On combining ^{1}H-MRS with conventional and other advanced MR imaging techniques such as perfusion MR imaging, grading becomes more precise. Some features of tumors on conventional MR imaging (eg, contrast enhancement, surrounding edema, signal heterogeneity, necrosis, hemorrhage, and midline crossing) and perfusion MR imaging (high rCBV) suggest a high grade. ^{1}H-MRS is complementary and helpful for glioma grading. High-grade gliomas demonstrate marked elevation of Cho, decreased NAA, and presence of Lac and lipids. Myo is high in low-grade gliomas and decreases with increasing grades of tumors.

An important issue regarding postradiation therapy in patients with brain tumors is differentiation between recurrent brain tumor and radiation injury/change, particularly when new contrast-enhancing lesions are seen in previously operated and/or irradiated regions. Many studies have found that Cho/Cr and/or Cho/NAA ratios are significantly higher in recurrent tumor (or predominantly tumor) than in radiation injury (**Fig. 13**).[54–57]

One study[57] reported that the Lac/Cr ratio was significantly higher in recurrent tumor than in radiation injury, whereas the lipid/Cr ratio was significantly lower in recurrent tumor than in radiation injury. Another study showed that the Lac or lipid signal alone was not helpful in differentiating these 2 conditions.[56] Rabinov and colleagues[54] have also demonstrated no correlation between the signal intensity of lipids and the histopathology, but they observed that the signal intensity of Lac in 2 patients with enhancing areas corresponded to recurrent tumor. It is probable that the amount of lipids may be higher in an area of radiation changes than in tumor recurrence, whereas Lac may be found in recurrent tumor, but both lipids and Lac cannot differentiate these conditions.

Infections

Distinguishing brain abscesses from necrotic brain tumors can be difficult on computed tomography or conventional MR imaging; these can appear as rim-enhancing lesions. Although pyogenic brain abscesses show restricted diffusion and brain tumors usually do not show the restriction, in some instances neoplasms may have restricted diffusion. ^{1}H-MRS may be helpful for establishing the diagnosis. In pyogenic abscess, typical ^{1}H-MRS spectra of the enhancing rim demonstrate a decrease in NAA and Cr levels but no change or a slight decrease in Cho level.[58,59] In one study,[35] maximum Cho/Cr, Cho/NAA, and Cho/Cho ratios in glioblastomas multiforme were significantly higher than in brain abscesses; thus, an increased Cho level specifies brain tumors.

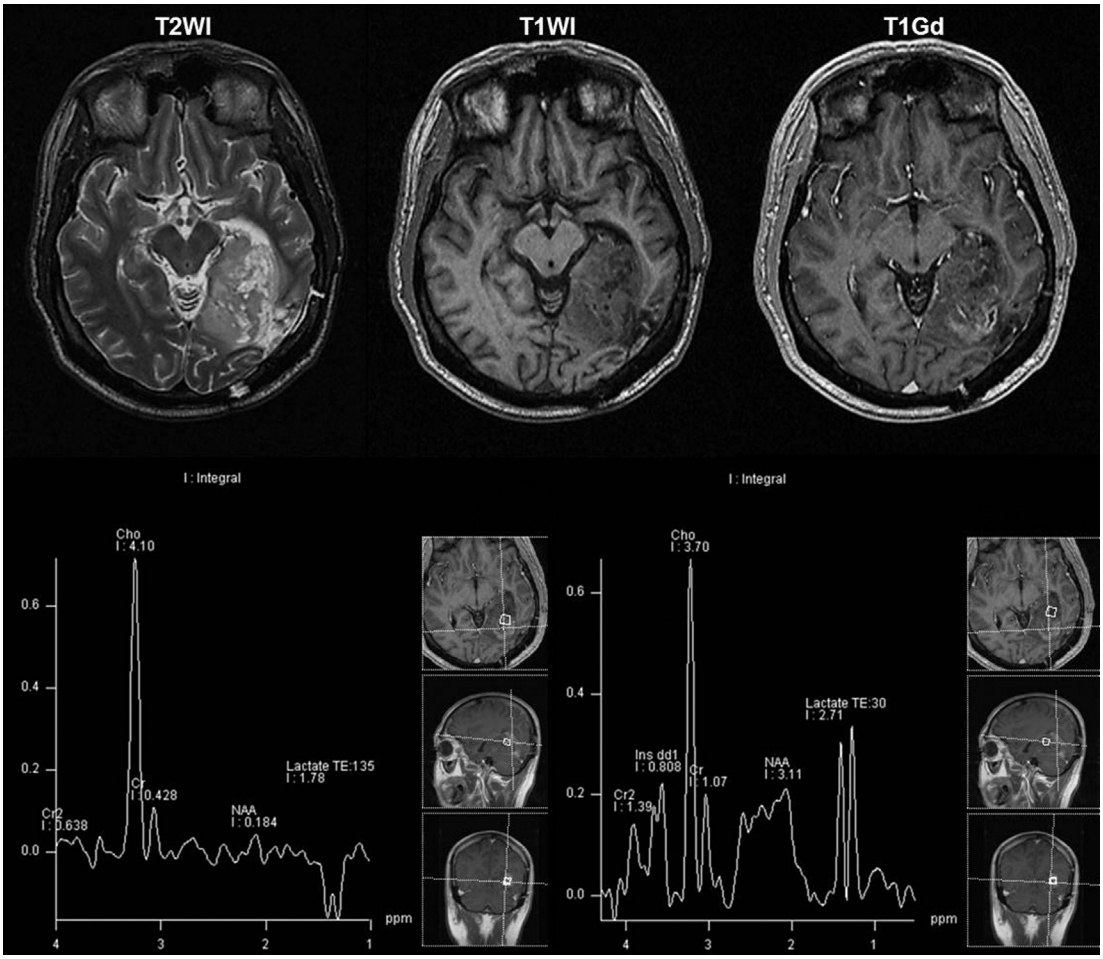

Fig. 13. Glioblastoma multiforme in deep portions of the left temporal and occipital lobes previously treated with surgery and radiotherapy. An area of irregular and patchy contrast enhancement is seen on the region of prior surgery that could correspond to tumor recurrence or treatment-induced changes. ^{1}H-MRS image shows high peak of Cho (and high Cho/Cr) and low NAA in all voxels of the grid (2 are shown), a pattern that is consistent with tumor recurrence. The presence of lactate could reflect tumor ischemia, but may be seen after treatment and thus its meaning is not clear. After treatment, the presence of lactate may signify treatment-induced necrosis and not high histologic grade. Cho, choline; Cr and Cr2, creatine; NAA, *N*-acetylaspartate; T1Gd, T1-weighted with gadolinium; T1WI, T1-weighted; T2WI, T2-weighted.

Spectra of the cystic portion of necrotic tumor or abscess cavity show a Lac peak and may show lipid signals, therefore Lac and lipid peaks are nonspecific.[35,37] By contrast, abscess demonstrates elevation of acetate, succinate, and some amino acids (eg, valine, leucine, and Ala), which are specific spectra and are not seen in the neoplasms.[35–37] However, there are 2 situations that one must be aware of. First, the resonances of acetate, succinate, and amino acids may be absent in an abscess under effective antibiotic therapy. Second, in aerobic bacterial abscesses, acetate is usually not present. Moreover, typical spectra of anaerobic bacterial abscesses (acetate, succinate, and amino acids) do not exist in *Staphylococcus aureus* abscess, which is one of the aerobic bacterial abscesses.[35] Therefore, interpretation of ^{1}H-MRS spectra of the enhancing rim along with the spectra of cystic components of the rim-enhancing lesions could differentiate anaerobic and aerobic bacterial abscesses, and necrotic brain tumors from each other.

Another challenge is discriminating between toxoplasmosis and lymphoma in human immunodeficiency virus infection. Both can have the appearance of rim-enhancing lesions. Lymphoma typically demonstrates restricted diffusion; however, toxoplasmosis has a variation of the diffusion and may overlap with that of the lymphoma.[60] Typical MR perfusion of lymphoma shows elevation

of rCBV, whereas toxoplasmosis does not. Positive findings using single-photon emission computed tomography and positron emission tomography (PET) are found in lymphoma.[61] On ^{1}H-MRS, lymphoma has an elevated Cho level. Toxoplasmosis shows lipid and Lac peaks, but these peaks are rather nonspecific and can be found in the necrotic portion of lymphoma.[61] A moderate decrease in NAA and a moderate increase in Cho have been documented in toxoplasmosis as well.[62]

Herpes simplex encephalitis is the most common encephalitis, which has typical distribution of brain involvement at the hippocampus and cortex of temporal, frontobasal, and insular lobes.[63] ^{1}H-MRS shows marked reduction of NAA and NAA/Cr ratio, and elevation of Cho and Cho/Cr ratio at the involved region, which reflect neuronal loss and gliosis and correlate with histopathologic findings.[63–65]

Inborn Error of Metabolism

The diagnosis of an inborn error of metabolism is always challenging and is mainly based on clinical and laboratory findings, evolution, and genetic tests. Brain MR imaging may help to narrow the differential diagnosis, avoid expensive genetic tests, or even establish a final diagnosis. Because these disorders are caused by inherited enzymatic defects, concentrations of some metabolites may be abnormally low or high. Metabolites with a very small concentration in brain tissue are not depicted on ^{1}H-MRS. In these cases, the changes in the spectrum usually correspond to a general abnormality, such as demyelination or ischemia. For some diseases, however, ^{1}H-MRS may identify a specific biomarker that helps in the diagnosis.[66]

Disorders that have specific ^{1}H-MRS patterns may manifest as an increase, decrease, or absence of particular metabolites. Specific biomarkers can be seen in phenylketonuria (phenylalanine), Canavan disease (NAA), nonketotic hyperglycinemia (glycine), creatine deficiency (Cr), and maple syrup urine disease (branched-chain amino acids and keto acids).[67]

Phenylalanine is an α-amino acid that is assigned at 7.36 ppm and can be used for the diagnosis of phenylketonuria, follow-up of treatment, and evolution of the disease. ^{1}H-MRS is usually not needed because early diagnosis is made by neonatal screening tests, and response to treatment can be monitored by phenylalanine blood levels and neuropsychological tests.

An increase in NAA signal is characteristic of Canavan disease (a disorder caused by a defect of the enzyme aspartoacylase that results in NAA accumulation in the brain) in a child with diffusely abnormal white matter and macrocephaly. However, a high peak at 2.03 ppm is also noted in Salla disease, a rare autosomal recessive free sialic acid storage disorder.[68] This latter disease accumulates acetylneuraminic acid (NANA), which resonates at the same frequency as NAA. In patients diagnosed with Pelizaeus-Merzbacher disease, the NAA peak may also be elevated.

Nonketotic hyperglycinemia is an autosomal recessive disease that manifests mainly during the neonatal period. There is accumulation of glycine in the brain, and this metabolite shows up in ^{1}H-MRS as a peak at 3.55 ppm. Of importance is that Myo resonates at 3.56 ppm, therefore these peaks overlap. However, glycine has a higher T2 value, and is seen with both short-TE and long-TE sequences.[66] Thus ^{1}H-MRS is an important tool for diagnosing nonketotic hyperglycinemia, and long-TE studies must be acquired. ^{1}H-MRS can also be used for monitoring the disease, correlating more with the clinical findings than levels of blood and cerebrospinal fluid glycine.

Maple syrup urine disease is an aminoacidopathy with accumulation of branched-chain α-keto and amino acids. These metabolites resonate at 0.9 ppm, a region that is usually attributed to lipids. Lac may also be present. In Cr deficiency there is a severe reduction in the Cr peak. In both diseases, ^{1}H-MRS may help with diagnosis and treatment.

All mitochondrial diseases caused by disorders of pyruvate metabolism, disorders of fatty acid oxidation, or defects of the respiratory chain and may show Lac elevation on ^{1}H-MRS. However, this finding is nonspecific and Lac is not always present. Nonetheless, in mitochondrial disorders an abnormal Lac peak may be present when the VOI is positioned in normal brain parenchyma on MR imaging and in the ventricles.[69,70] Therefore, even if the findings of ^{1}H-MRS are nonspecific, they may be useful in the evaluation of mitochondrial disorders.

Dementia

Dementia is a clinical diagnosis in patients with a decline in memory and cognitive function. MR imaging may play an important role in ruling out neurologic disorders that may clinically present with dementia, such as subdural hematomas, tumors, and multiple cerebral infarctions. The most common causes of dementia, however, are AD, dementia with Lewy bodies, and vascular dementia. Although there are clinical criteria to differentiate these pathologic subtypes of dementia, pathologic studies have shown that such criteria are not accurate. Therefore, specific imaging neuromarkers may help in the differential diagnosis.

In patients with dementia, ^{1}H-MRS may aid in the differential diagnosis and progression of the disease.[71] AD is associated with neuronal damage, particularly in the limbic cortical regions. In the end stages of the disease, primary sensorimotor and neuronal cortices are also involved. ^{1}H-MRS shows a reduction on NAA/Cr ratio and elevation of Myo/Cr ratio, especially in paralimbic cortical regions (posterior cingulate gyri).[72,73] The higher level of Myo is thought to be associated with gliosis.[74]

Mild cognitive impairment (MCI) is established as a transitional state between the cognitive changes of normal aging and AD.[75] Patients with MCI have memory loss, but still do not meet criteria for AD; however, they usually have AD pathology. This condition is suitable for early therapeutic intervention. ^{1}H-MRS depicts high Myo/Cr levels in the parietal lobes of these patients. NAA/Cr is either mildly decreased or normal.

^{1}H-MRS measurements of NAA and Myo levels are also a marker for progression of clinical disease, and correlate with dementia severity and neuropsychological cognitive function. A study comparing antemortem ^{1}H-MRS and neuropathologic criteria for AD demonstrated a strong association between NAA/Myo levels and disease progression.[76]

Seizures

Localization of the focus of an epileptogenic seizure relies on the combination of many different techniques, such as video-electroencephalography (EEG), neuropsychological assessment, and PET. MR imaging may also be useful in detecting the epileptic focus. MR imaging is usually performed in patients with recent-onset or recurring focal seizures. Underlying structural abnormalities, such as cortical dysplasia and tumors, are depicted on MR imaging and may be the cause of focal epilepsy. However, in some patients with focal epilepsy, MR imaging does not show any structural abnormality. The role of ^{1}H-MRS is to help characterize and localize the epileptogenic focus, especially when studying patients with refractory focal epilepsy and without clear MR imaging abnormalities.

Temporal lobe epilepsy (TLE) is the most common cause of focal epilepsy. Hippocampal sclerosis is responsible for most cases of TLE. The characteristic MR imaging findings are hippocampal increased T2-weighted signal, reduced volume, and architectural distortion. The accuracy of MR imaging to detect abnormalities in TLE is controversial. Studies[77,78] have indicated a high reliability in the diagnosis of hippocampal sclerosis using MR imaging, with sensitivity of up to 90% and specificity up to 70%. However, other studies showed that approximately 20% of patients with TLE have no findings on MR imaging.[79]

^{1}H-MRS may help to distinguish the side of the focus in some cases of TLE, particularly in patients with normal brain MR imaging.[71,80] A reduction in NAA concentration and NAA/Cho + Cr ratio is the typical abnormality of TLE, and is a reflection of neuronal damage.[81] Increased Cho and Myo signals may also be present, and are believed to be caused by gliosis. However, the specificity of the abnormal concentration of the metabolites on ^{1}H-MRS is unknown. Abnormalities on ^{1}H-MRS have been seen in both temporal lobes in patients with TLE.[71,79] Moreover, metabolic changes were also found in other areas distant to the seizure focus, probably due to widespread effects of seizures.[71] These ^{1}H-MRS abnormalities in distant areas may reverse after surgery.[82]

SUMMARY

MR spectroscopy offers a noninvasive means of assessing in vivo brain metabolites that shed light on cellular concentrations, cell function and dysfunction, cellular energetics, presence of ischemia, and presence of necrosis, among others. Studies obtained at higher field strengths are evolving toward sampling of smaller tissue volumes, greater SNR, and higher metabolic spatial resolution. From the clinical standpoint MR spectroscopy is useful in various disorders, as described in this review. However, to be valid and significant the results of MR spectroscopy should always be correlated with their imaging counterparts.

REFERENCES

1. Duyn JH, Moonen CT. Fast proton spectroscopic imaging of human brain using multiple spin-echoes. Magn Reson Med 1993;30:409–14.
2. Duyn JH, Gillen J, Sobering G, et al. Multisection proton MR spectroscopic imaging of the brain. Radiology 1993;188:277–82.
3. Posse S, DeCarli C, Le Bihan D. Three-dimensional echoplanar MR spectroscopic imaging at short echo times in the human brain. Radiology 1994; 192:733–8.
4. Ethofer T, Mader I, Seeger U, et al. Comparison of longitudinal metabolite relaxation times in different regions of the human brain at 1.5 and 3 Tesla. Magn Reson Med 2003;50:1296–301.
5. Fayed N, Olmos S, Morales H, et al. Physical basis of magnetic resonance spectroscopy and its application to central nervous system diseases. Am J Appl Sci 2006;3:1836–45.
6. Hajek M, Dezortova M. Introduction to clinical in vivo MR spectroscopy. Eur J Radiol 2008;67:185–93.

7. Soares DP, Law M. Magnetic resonance spectroscopy of the brain: review of metabolites and clinical applications. Clin Radiol 2009;64:12–21.
8. Mullins ME. MR spectroscopy: truly molecular imaging; past, present and future. Neuroimaging Clin N Am 2006;16:605–18.
9. van der Graaf M. In vivo magnetic resonance spectroscopy: basic methodology and clinical applications. Eur Biophys J 2010;39:527–40.
10. Charles HC, Lazeyras F, Krishnan KR, et al. Proton spectroscopy of human brain: effects of age and sex. Prog Neuropsychopharmacol Biol Psychiatry 1994;18:995–1004.
11. Nagae-Poetscher LM, Bonekamp D, Barker PB, et al. Asymmetry and gender effect in functionally lateralized cortical regions: a proton MRS imaging study. J Magn Reson Imaging 2004;19:27–33.
12. Hetherington HP, Mason GF, Pan JW, et al. Evaluation of cerebral gray and white matter metabolite differences by spectroscopic imaging at 4.1T. Magn Reson Med 1994;32:565–71.
13. Kreis R, Ernst T, Ross BD. Absolute quantitation of water and metabolites in the human brain. II. Metabolite concentrations. J Magn Reson B 1993;102:9–19.
14. Soher BJ, van Zijl PC, Duyn JH, et al. Quantitative proton MR spectroscopic imaging of the human brain. Magn Reson Med 1996;35:356–63.
15. Degaonkar MN, Pomper MG, Barker PB. Quantitative proton magnetic resonance spectroscopic imaging: regional variations in the corpus callosum and cortical gray matter. J Magn Reson Imaging 2005;22:175–9.
16. Pouwels PJ, Frahm J. Regional metabolite concentrations in human brain as determined by quantitative localized proton MRS. Magn Reson Med 1998; 39:53–60.
17. Baker EH, Basso G, Barker PB, et al. Regional apparent metabolite concentrations in young adult brain measured by (1)H MR spectroscopy at 3 Tesla. J Magn Reson Imaging 2008;27:489–99.
18. Jacobs MA, Horská A, van Zijl PC, et al. Quantitative proton MR spectroscopic imaging of normal human cerebellum and brain stem. Magn Reson Med 2001; 46:699–705.
19. Arslanoglu A, Bonekamp D, Barker PB, et al. Quantitative proton MR spectroscopic imaging of the mesial temporal lobe. J Magn Reson Imaging 2004;20:772–8.
20. Vermathen P, Laxer KD, Matson GB, et al. Hippocampal structures: anteroposterior N-acetylaspartate differences in patients with epilepsy and control subjects as shown with proton MR spectroscopic imaging. Radiology 2000;214:403–10.
21. Dezortova M, Hajek M. (1)H MR spectroscopy in pediatrics. Eur J Radiol 2008;67:240–9.
22. Kreis R, Ernst T, Ross BD. Development of the human brain: In vivo quantification of metabolite and water content with proton magnetic resonance spectroscopy. Magn Reson Med 1993;30:424–37.
23. Christiansen P, Toft P, Larsson HB, et al. The concentration of N-acetyl aspartate, creatine + phosphocreatine, and choline in different parts of the brain in adulthood and senium. Magn Reson Imaging 1993;11:799–806.
24. Lim KO, Spielman DM. Estimating NAA in cortical gray matter with applications for measuring changes due to aging. Magn Reson Med 1997;37:372–7.
25. Chang L, Ernst T, Poland RE, et al. In vivo proton magnetic resonance spectroscopy of the normal aging human brain. Life Sci 1996;58:2049–56.
26. Haga KK, Khor YP, Farrall A, et al. A systemic review of brain metabolite changes, measured with (1)H magnetic resonance spectroscopy, in healthy aging. Neurobiol Aging 2009;30:353–63.
27. Majós C, Julià-Sapé M, Alonso J, et al. Brain tumor classification by proton MR spectroscopy: comparison of diagnostic accuracy at short and long TE. AJNR Am J Neuroradiol 2004;10:1696–704.
28. Gupta, Rakesh K. Relationships between choline magnetic resonance spectroscopy, apparent diffusion coefficient and quantitative histopathology in human glioma. Journal of Neuro-oncology 2000; 50(3):215–26.
29. Majós C, Aguilera C, Alonso J, et al. Proton MR spectroscopy improves discrimination between tumor and pseudotumoral lesion in solid brain masses. AJNR Am J Neuroradiol 2009;30(3):544–51.
30. Vuori K, Kankaanranta L, Häkkinen AM, et al. Low-grade gliomas and focal cortical developmental malformations: differentiation with proton MR spectroscopy. Radiology 2004;230(3):703–8.
31. Bitsch A, Bruhn H, Vougioukas V, et al. Inflammatory CNS demyelination: histopathologic correlation with in vivo quantitative proton MR spectroscopy. AJNR Am J Neuroradiol 1999;20(9):1619–27.
32. De Stefano N, Filippi M, Miller D, et al. Guidelines for using proton MR spectroscopy in multicenter clinical MS studies. Neurology 2007;69(20):1942–52.
33. Srinivasan R, Sailasuta N, Hurd R, et al. Evidence of elevated glutamate in multiple sclerosis using magnetic resonance spectroscopy at 3 T. Brain 2005;128(Pt 5):1016–25.
34. Fernando KT, McLean MA, Chard DT, et al. Elevated white matter myo-inositol in clinically isolated syndromes suggestive of multiple sclerosis. Brain 2004;127(Pt 6):1361–9.
35. Lai PH, Weng HH, Chen CY, et al. In vivo differentiation of aerobic brain abscesses and necrotic glioblastomas multiforme using proton MR spectroscopic imaging. AJNR Am J Neuroradiol 2008;29(8):1511–8.
36. Grand S, Passaro G, Ziegler A, et al. Necrotic tumor versus brain abscess: importance of amino acids detected at ^{1}H MR spectroscopy–initial results. Radiology 1999;213(3):785–93.

37. Lai PH, Ho JT, Chen WL, et al. Brain abscess and necrotic brain tumor: discrimination with proton MR spectroscopy and diffusion-weighted imaging. AJNR Am J Neuroradiol 2002;23(8):1369–77.
38. Law M, Cha S, Knopp EA, et al. High-grade gliomas and solitary metastases: differentiation by using perfusion and proton spectroscopic MR imaging. Radiology 2002;222(3):715–21.
39. Cohen BA, Knopp EA, Rusinek H, et al. Assessing global invasion of newly diagnosed glial tumors with whole-brain proton MR spectroscopy. AJNR Am J Neuroradiol 2005;26(9):2170–7.
40. Stadlbauer A, Gruber S, Nimsky C, et al. Preoperative grading of gliomas by using metabolite quantification with high-spatial-resolution proton MR spectroscopic imaging. Radiology 2006;238(3):958–69.
41. Hollingworth W, Medina LS, Lenkinski RE, et al. A systematic literature review of magnetic resonance spectroscopy for the characterization of brain tumors. AJNR Am J Neuroradiol 2006;27(7):1404–11.
42. Law M, Yang S, Wang H, et al. Glioma grading: sensitivity, specificity, and predictive values of perfusion MR imaging and proton MR spectroscopic imaging compared with conventional MR imaging. AJNR Am J Neuroradiol 2003;24(10):1989–98.
43. Castillo M, Smith JK, Kwock L. Correlation of myo-inositol levels and grading of cerebral astrocytomas. AJNR Am J Neuroradiol 2000;21(9):1645–9.
44. Howe FA, Barton SJ, Cudlip SA, et al. Metabolic profiles of human brain tumors using quantitative in vivo ^{1}H magnetic resonance spectroscopy. Magn Reson Med 2003;49(2):223–32.
45. Tedeschi G, Lundbom N, Raman R, et al. Increased choline signal coinciding with malignant degeneration of cerebral gliomas: a serial proton magnetic resonance spectroscopy imaging study. J Neurosurg 1997;87(4):516–24.
46. Taillibert S, Chodkiewicz C, Laigle-Donadey F, et al. Gliomatosis cerebri: a review of 296 cases from the ANOCEF database and the literature. J Neurooncol 2006;76(2):201–5.
47. Galanaud D, Chinot O, Nicoli F, et al. Use of proton magnetic resonance spectroscopy of the brain to differentiate gliomatosis cerebri from low-grade glioma. J Neurosurg 2003;98(2):269–76.
48. David NL, Hiroko O, Otmar D, et al. The 2007 WHO Classification of Tumours of the Central Nervous System. Acta Neuropathol 2007;114(2):97–109.
49. Lev MH, Ozsunar Y, Henson JW, et al. Glial tumor grading and outcome prediction using dynamic spin-echo MR susceptibility mapping compared with conventional contrast-enhanced MR: confounding effect of elevated rCBV of oligodendrogliomas [corrected]. AJNR Am J Neuroradiol 2004;25(2):214–21.
50. Cha S, Tihan T, Crawford F, et al. Differentiation of low-grade oligodendrogliomas from low-grade astrocytomas by using quantitative blood-volume measurements derived from dynamic susceptibility contrast-enhanced MR imaging. AJNR Am J Neuroradiol 2005;26(2):266–73.
51. Xu M, See SJ, Ng WH, et al. Comparison of magnetic resonance spectroscopy and perfusion-weighted imaging in presurgical grading of oligodendroglial tumors. Neurosurgery 2005;56(5):919–26 [discussion: 919–26].
52. Spampinato MV, Smith JK, Kwock L, et al. Cerebral blood volume measurements and proton MR spectroscopy in grading of oligodendroglial tumors. AJR Am J Roentgenol 2007;188(1):204–12.
53. Rijpkema M, Schuuring J, van der Meulen Y, et al. Characterization of oligodendrogliomas using short echo time ^{1}H MR spectroscopic imaging. NMR Biomed 2003;16(1):12–8.
54. Rabinov JD, Lee PL, Barker FG, et al. In vivo 3-T MR spectroscopy in the distinction of recurrent glioma versus radiation effects: initial experience. Radiology 2002;225(3):871–9.
55. Smith EA, Carlos RC, Junck LR, et al. Developing a clinical decision model: MR spectroscopy to differentiate between recurrent tumor and radiation change in patients with new contrast-enhancing lesions. AJR Am J Roentgenol 2009;192(2):W45–52.
56. Weybright P, Sundgren PC, Maly P, et al. Differentiation between brain tumor recurrence and radiation injury using MR spectroscopy. AJR Am J Roentgenol 2005;185(6):1471–6.
57. Zeng QS, Li CF, Liu H, et al. Distinction between recurrent glioma and radiation injury using magnetic resonance spectroscopy in combination with diffusion-weighted imaging. Int J Radiat Oncol Biol Phys 2007;68(1):151–8.
58. Burtscher IM, Holtas S. In vivo proton MR spectroscopy of untreated and treated brain abscesses. AJNR Am J Neuroradiol 1999;20:1049–53.
59. Remy C, Grand S, Lai ES, et al. ^{1}H MRS of human brain abscess in vivo and in vitro. Magn Reson Med 1995;34:508–14.
60. Schroeder PC, Post MJ, Orchatz E, et al. Analysis of the utility of diffusion-weighted MRI and apparent diffusion coefficient values in distinguishing central nervous system toxoplasmosis from lymphoma. Neuroradiology 2006;48:715–20.
61. Pomper MG, Constantinides CD, Barker PB, et al. Quantitative MR spectroscopic imaging of brain lesions in patients with AIDS: correlation with [^{11}C-methyl]thymidine PET and thallium-201 SPECT. Acad Radiol 2002;9:398–409.
62. Ionita C, Wasay M, Balos L, et al. MR imaging in toxoplasmosis encephalitis after bone marrow transplantation: paucity of enhancement despite fulminant disease. AJNR Am J Neuroradiol 2004;25:270–3.

63. Samann PG, Schlegel J, Muller G, et al. Serial proton MR spectroscopy and diffusion imaging findings in HIV-related herpes simplex encephalitis. AJNR Am J Neuroradiol 2003;24:2015–9.
64. Hitosugi M, Ichijo M, Matsuoka Y, et al. Proton MR spectroscopy findings in herpes simplex encephalitis. Rinsho Shinkeigaku 1996;36:839–43.
65. Takanashi J, Sugita K, Ishii M, et al. Longitudinal MR imaging and proton MR spectroscopy in herpes simplex encephalitis. J Neurol Sci 1997;149:99–102.
66. Barker PB, Bizzi A, De Stefano N, et al. Clinical MR spectroscopy. 1st edition. New York: Cambridge University Press; 2010. ISBN 9780521868983.
67. van der Knaap MS, Valk J. Magnetic resonance of myelin disorders. 3rd edition. Heidelberg (Germany): Springer; 2005. ISBN 13:9783540222866.
68. Varho T, Komu M, Sonninen P, et al. A new metabolite contributing to N-acetyl signal in ^{1}H MRS of the brain in Salla disease. Neurology 1999;52(8):1668–72.
69. Bianchi MC, Tosetti M, Battini R, et al. Proton MR spectroscopy of mitochondrial diseases: analysis of brain metabolic abnormalities and their possible diagnostic relevance. AJNR Am J Neuroradiol 2003;24(10): 1958–66.
70. Cross JH, Gadian DG, Connelly A, et al. Proton magnetic resonance spectroscopy studies in lactic acidosis and mitochondrial disorders. J Inherit Metab Dis 1993;16(4):800–11.
71. Gillard JH, Waldman AD, Barker PB. Clinical MR neuroimaging: physiological and functional techniques. 2nd edition. New York: Cambridge University Press; 2010. ISBN 9780521515634.
72. Huang W, Alexander GE, Chang L, et al. Brain metabolite concentration and dementia severity in Alzheimer's disease: a (1)H MRS study. Neurology 2001;57(4):626–32.
73. Miller BL, Moats RA, Shonk T, et al. Alzheimer disease: depiction of increased cerebral myo-inositol with proton MR spectroscopy. Radiology 1993;187(2): 433–7.
74. Ross BD, Bluml S, Cowan R, et al. In vivo MR spectroscopy of human dementia. Neuroimaging Clin N Am 1998;8(4):809–22.
75. Petersen RC, Doody R, Kurz A, et al. Current concepts in mild cognitive impairment. Arch Neurol 2001;58(12):1985–92.
76. Kantarci K, Knopman DS, Dickson DW, et al. Alzheimer disease: postmortem neuropathologic correlates of antemortem ^{1}H MR spectroscopy metabolite measurements. Radiology 2008;248(1): 210–20.
77. Lee DH, Gao FQ, Rogers JM, et al. MR in temporal lobe epilepsy: analysis with pathologic confirmation. AJNR Am J Neuroradiol 1998;19:19–27.
78. Park SW, Chang KH, Kim HD, et al. Lateralizing ability of single-voxel proton MR spectroscopy in hippocampal sclerosis: comparison with MR imaging and positron emission tomography. AJNR Am J Neuroradiol 2001;22:625–31.
79. Connelly A, van Paesschen W, Porter DA, et al. Proton magnetic resonance spectroscopy in MRI-negative temporal lobe epilepsy. Neurology 1998; 51(1):61–6.
80. Doelken MT, Stefan H, Pauli E, et al. (1)H-MRS profile in MRI positive versus MRI negative patients with temporal lobe epilepsy. Seizure 2008;17:490–7.
81. Najm IM, Wang Y, Shedid D, et al. MRS metabolic markers of seizures and seizure-induced neuronal damage. Epilepsia 1998;39(3):244–50.
82. Serles W, Li LM, Antel SB, et al. Time course of postoperative recovery of N-acetyl-aspartate in temporal lobe epilepsy. Epilepsia 2001;42(2):190–7.